(Received 7 October 2023, Accepted 7 December 2023, Scheduled 18 December 2023)

A Quad-Band High-Isolated MIMO Microstrip Antenna for Coal Mine Communication

Yanhong Xu[1, *], Peipei Dong[1], Anyi Wang[1], Jianqiang Hou[2], and Shanshan Li[3]

[1] *Xi'an Key Laboratory of Network Convergence Communication, College of Communication and Information Engineering Xi'an University of Science and Technology, Xi'an 710054, China*
[2] *National Key Laboratory of Science and Technology on Antenna and Microwave, Xidian University, Xi'an 710071, China*
[3] *Xi'an Dolphin Radar Science and Technology LTD, Xi'an 710065, China*

ABSTRACT: In this letter, a quad-band high-isolated MIMO microstrip antenna is designed for coal mine communications, which can operate at DCS1800, UMTS, WiMAX, WiFi, and 5G NR simultaneously. Firstly, the qual-band property is realized by designing a quaddent structure. In particular, three L-shaped branches (separately operating at 2.6 GHz, 3.5 GHz, and 4.8 GHz) are successively loaded on a monopole antenna (operating at 1.9 GHz). In the sequel, by symmetrically placing two quaddent structures with spacing of 0.19λ, a MIMO antenna is designed. At this time, the isolation level of the MIMO antenna can be as high as around 8 dB. To improve the performance of the MIMO antenna, an inverted cross-shaped branch is loaded on and two rectangular slots are etched off the ground successively between the two elements. In this way, an isolation level of over 20 dB can be achieved across the whole operating frequency bands. To verify the performance of the designed antenna, a prototype is fabricated and tested, and good agreement between the simulated and measured results indicates that the proposed antenna can completely cover DCS1800, UMTS, WiMAX, WiFi, and 5G NR ($1.67 \sim 2.28$ GHz, $2.39 \sim 2.79$ GHz, $3.13 \sim 3.74$ GHz and $4.69 \sim 5.34$ GHz) for mining.

1. INTRODUCTION

With the rapid development of wireless communication, people have stronger demands for channel capacity and transmission rate. 5G technique [1–3] is employed in coal mine applications owing to possessing the above advantages. Multiple-input multiple-output (MIMO) technology, as the key technology of 5G, is able to enhance channel capacity, spectrum utilization and reliability of the communication system via using multiple antennas technology at the transmitter and receiver with a little transmission power and bandwidth [4–6]. Especially, it plays an important role under the complex coal mine wireless environment. Physical channels exhibit randomly time-varying characteristics, which will result in signal fading and substantial channel capacity degradation [7]. However, the spacing between antenna elements will reduce if multiple antennas are arranged in the limited communication equipment, which would cause strong coupling between antenna units. Eventually, the radiation performance and channel capacity will be affected seriously due to the harmful coupling [8]. Therefore, researchers from both industry and academia have been focusing on how to achieve reduction of the coupling effect among MIMO antenna elements.

In recent years, many investigations have been conducted to reduce the coupling effects among MIMO antenna units. In [9, 10], spatial decoupling method is used by orthogonally placing the antenna units to reduce the coupling. The method is simple but occupies large system space. Another two decoupling techniques, i.e., neutralization line [11–13] and parasitic branch [14–16], use the principle of current cancellation to achieve decoupling and are more suitable for bandwidth decoupling. In particular, in [12], the isolation of the proposed antenna is more than 15 dB via using a T-shaped neutralization line with two Y-shaped stubs. In [15], a high isolation of better than 23 dB over 3.08–12.8 GHz is realized by adding inverted L-structured stubs on the ground plane. Loading metasurface structure [17, 18] and adopting differential feed [19, 20] are also exploited to reduce the coupling effect. In [18], a decoupling method of the metasurface-based is employed to realize the isolation of greater than 25 dB within the operating frequency bands. In [20], a differential-fed scheme is used to excite the y-polarization modes, which can obtain the isolation of higher than 48 dB within the whole band. Although the isolation can be greatly improved with the two methods, the difficulties in design and fabrication are also increased. Defective ground structures (DGS) and parasitic branches are combined to achieve reduction of the mutual coupling [21–23]. In [21], a wideband MIMO antenna is proposed by using a parasitic strip and DGS simultaneously to realize broadband and high isolation. Similarly, a dual-band MIMO antenna is proposed where an isolation of more than 15 dB is realized in the 2.4–2.48 and 5.15–5.825 GHz bands by firstly etching an inverted T-slot on the ground and then loading a meandering resonant branch [22]. It is obvious that the decoupling method is suitable for not only wideband but also multi-band antennas.

* Corresponding author: Yanhong Xu (yanhongxuxidian@163.com).

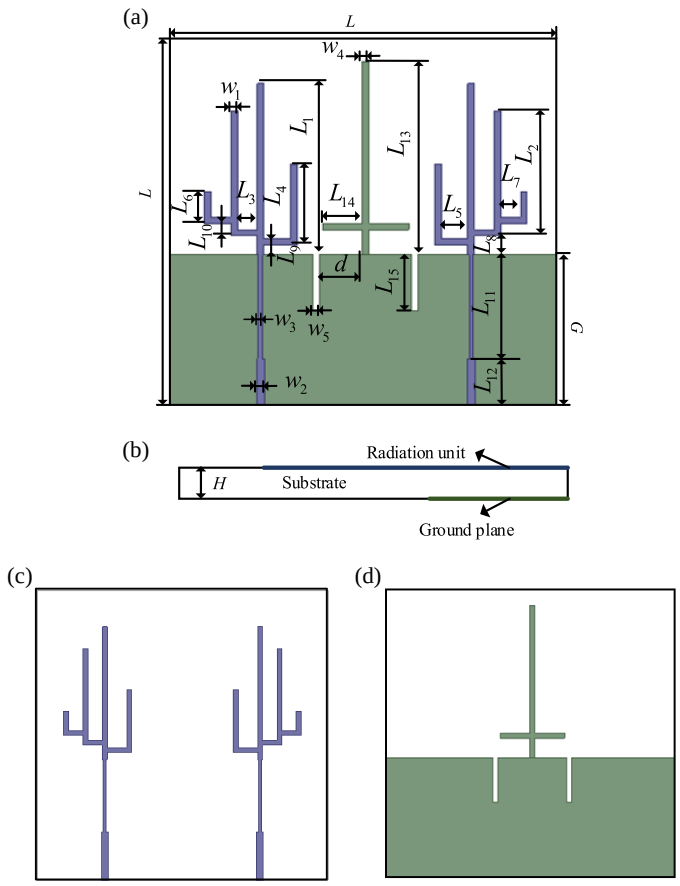

FIGURE 1. (a) The double-sided view. (b) Left side view. (c) Upper side view. (d) Lower side view (with $L_1 = 27.5$, $L_2 = 20$, $L_3 = 3$, $L_4 = 13$, $L_5 = 4$, $L_6 = 5$, $L_7 = 3$, $L_8 = 3$, $L_9 = 1.5$, $L_{10} = 2$, $L_{11} = 17$, $L_{12} = 8$, $L_{13} = 31$, $L_{14} = 5$, $L_{15} = 9$, $d = 6.5$, $w_1 = 1$, $w_2 = 1.2$, $w_3 = 0.6$, $w_4 = 1$, $w_5 = 1$, $L = 60$, $G = 25$, $H = 0.8$, in mm).

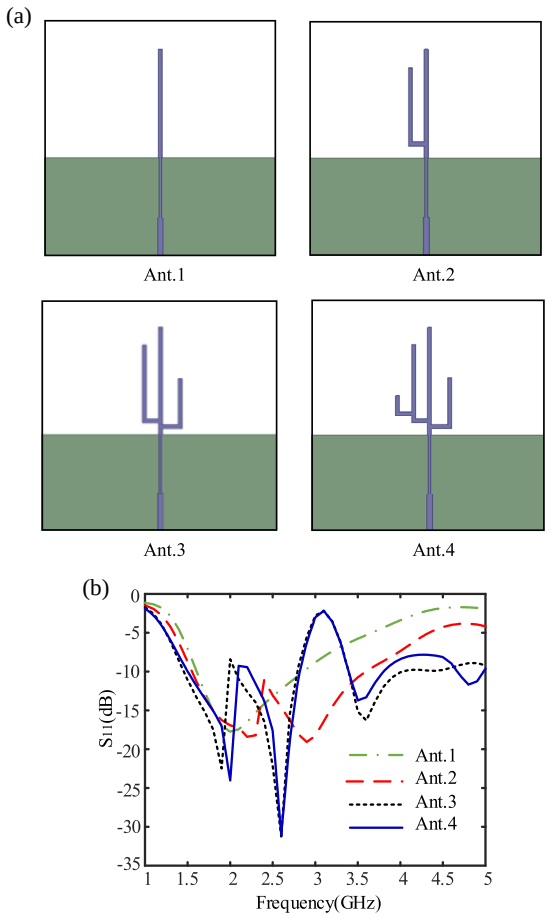

FIGURE 2. (a) Design procedures of the quad-band antenna. (b) The S_{11}-parameter curves of the quad-band antenna.

At present, the coexistence of multiple communication systems is prominent in the equipment under coal mine. As has been described above, the 5G technology is gradually applied in coal mine. An antenna, as the front end of an equipment, which can operate at 5G NR (2.51–2.67, 3.4–3.6, 4.8–4.9 GHz) and the previous frequency regions simultaneously, is prevailing from the perspective of saving space. Under this circumstance, a tri-band MIMO antenna for coal mine application is designed which can not only achieve the coverage of 5G NR, 4G, WiFi, and WiMAX frequency bands, but also provide a large channel capacity [23]. On this basis, a quad-band MIMO antenna is proposed for coal mine wireless communication in this letter which can achieve four frequency characteristics, i.e., $1.67 \sim 2.28$, $2.39 \sim 2.79$, $3.13 \sim 3.74$, and $4.69 \sim 5.34$ GHz. The proposed antenna can complete coverage of the commercial 5G NR spectrum ($2.51 \sim 2.67$, $3.40 \sim 3.60$, $4.80 \sim 4.90$ GHz), DCS1800 ($1.71 \sim 1.88$ GHz), UMTS ($1.92 \sim 2.17$ GHz), WiFi ($2.40 \sim 2.48$ GHz), and WiMAX ($2.5 \sim 2.69$ GHz), simultaneously. The isolation of the entire frequency regions is higher than 20 dB by loading an inverted cross-shaped branch on and etching two rectangular slots out of the ground successively between two antenna elements.

2. ANTENNA DESIGN

2.1. Structure of the Proposed MIMO Antenna

The double-sided view and left side view of the proposed antenna are displayed in Figures 1(a) and (b). The antenna consists of radiation units, dielectric substrate, ground plane, and decoupling structures. Figures 1(c) and (d) present the upper and lower side views of the dielectric substrate, respectively. Two symmetrical radiation units are located on the side of a 0.8 mm-thick FR4 substrate. The radiation units consist of radiation branches, impedance converters, and 50 Ω microstrip lines to form quaddent antennas. The ground plane is set beneath the dielectric substrate. Decoupling structures are arranged between two antenna units via loading an inverted cross-shaped branch on and etching two rectangular slots out of the ground. Figure 1 provides the optimized parameters of antenna.

2.2. Design of Quad-Band Element

Firstly, a quaddent antenna is designed to achieve four frequency characteristics, i.e., 1.50–2.09, 2.23–2.82, 3.39–3.80, and 4.67–5.00 GHz, which can realize the coverage of 5G NR, DCS1800, WiFi, and WiMAX frequency bands, simultaneously. The quad-band element is achieved by successively loading three L-shaped branches (separately operating at 2.6 GHz, 3.5 GHz, and 4.8 GHz) on a monopole antenna (operating at 1.9 GHz). The developing procedures of the quad-band element are provided in Figure 2(a), and Figure 2(b) gives the S_{11} parameter curves of the quad-band element. There are four steps in total. Step 1: antenna 1 (Ant. 1), a monopole antenna operating at the frequency band of 1.61–2.86 GHz is set in the middle of the substrate. Step 2: the first L-shaped branch is loaded on the left side of the monopole antenna to obtain antenna 2 (Ant. 2), which results in the second operating frequency region, i.e., 2.40–3.61 GHz. Step 3: antenna 3 (Ant. 3), the second L-shaped branch is loaded on the right side of the monopole antenna to generate a new operating frequency band of 3.39–4.03 GHz. Step 4: the third L-shaped branch, which is introduced to produce the fourth operating frequency band, i.e., 4.67–5.00 GHz, is placed on the outside of the first L-shaped branch to get antenna 4 (Ant. 4). Finally, the quad-band antenna operates at 1.50–2.09, 2.23–2.82, 3.39–3.80, and 4.67–5.00 GHz, which enable the quad-band antenna to complete the coverage of 5G NR/DCS1800/WiFi/WiMAX frequency bands, simultaneously.

2.3. Design of Quad-Band MIMO Antenna with High Isolation

In the sequel, the MIMO antenna is arranged by symmetrically placing two quaddent structures with spacing of 0.19λ (λ is the wavelength at 1.9 GHz). Generally speaking, when multiple antennas are placed in a space less than $\lambda/2$, mutual coupling will seriously affect the radiation performance and channel capacity of the antenna. To improve the isolation level, it is necessary to introduce decoupling structures, i.e., load an inverted cross-shaped branch on the ground, and then etch two rectangular slots out of the ground between two antenna units. The S_{21}-parameter curves and the developing procedures of the quad-band MIMO antenna decoupling are provided in Figures 3(a) and (b). As depicted in Figures 3(a) and (b), it can be observed that the isolation of the antenna is around 8 dB before decoupling, while the isolation of the whole frequency regions is higher than 20 dB after adding decoupling structures.

As an illustration of decoupling principle, the simulated current distributions of the proposed quad-band MIMO antenna at 1.9, 2.6, 3.5, and 4.8 GHz are presented in Figure 3(c). Note that excite the left port while connect a matching load to the right port. Before adding decoupling structures, it is observed that strong current on the unit 1 is coupled to unit 2 at the four frequencies. Loading an inverted cross-shaped branch on the ground is implemented firstly. Part of the strong current is coupled on an inverted cross-shaped branch at 1.9, 3.5 and 4.8 GHz, which can also further couple energy to unit 2. The current coupled by unit 1 to unit 2 can be partially cancelled by the current coupled by the inverted cross-shaped branch on unit 2 via appropriately selecting the parameters of the inverted cross-shaped branch. Etching two rectangular slots out of the ground is further conducted. Part of the strong current is excited on the left slot at four frequencies, which can also couple current on unit 2. The current coupled by unit 1 on unit 2 can be further neutralized by this current coupled by the rectangular slots on unit 2. The resultant current on unit 2 can be further reduced via properly choosing the structure parameters of the rectangular slots, finally improving the isolation level between two ports.

The parametric analysis of the decoupling structure is given below for four parameters, i.e., L_{13}, L_{14}, w_4, and L_{15}. The effects of the above four parameters on S_{21} are shown in Figure 4. Among them, L_{13}, L_{14}, and w_4 are the main parameters of the inverted cross-shaped branch. As shown in Figure 4(a), it can be seen that the values of S_{21} at the first and third frequency bands are more affected with the change of L_{13}. The values of S_{21} at some parts of the first frequency region are reduced, but others increased, and reduced at the third frequency band with the growth of L_{13}. To compromise, L_{13} is determined as 31 mm finally. Figure 4(b) provides the effects of the L_{14} on S_{21}. The values of S_{21} at the third frequency region are mainly affected with the growth of L_{14}. The values of S_{21} are reduced at the third frequency regions and then increased along with the growth of L_{14}. To achieve high isolation, L_{14} is determined as 6.5 mm finally. As shown in Figure 4(c), it can be observed that the values of S_{21} at the first and third frequency regions are easily affected with the growth of w_4. With the growth of w_4, the values of S_{21} are reduced at the first frequency region but reduced and then increased at the third frequency region. For the sake of a good isolation level, w_4 is determined as 1.0 mm. From Figure 4(d), it is seen that the values of S_{21} at the first, third, and fourth frequency regions are affected obviously with the growth of L_{15}. The change of S_{21} at the first frequency region is similar to the investigation of L_{13}, while the values of S_{21} are reduced and then increased at the third and fourth frequency regions with the growth of L_{15}. Therefore, L_{15} is finally determined as 9.0 mm.

3. SIMULATED AND MEASURED RESULTS

To validate our work, a prototype of the proposed antenna is provided in Figure 5(a). The prototype of the proposed MIMO antenna is measured in an anechoic chamber. During the measurement, the prototype is placed on a turntable, and a standard horn antenna, termed as horn 1, is utilized as the receiver at the same horizontal level in the far-field region of the prototype. The measured results are acquired by applying an Agilent N5244A network analyzer. Figure 5(b) provides the curves of the simulated and measured S-parameters. It can be seen that the measured values agree well with the simulated results. According to the measured results, it can be observed that the coupling between antenna units is greatly reduced by introducing decoupling structures. In particular, the values of S_{21} are lower than -20, -21, -23, and -30 dB at four frequency regions of $1.67 \sim 2.28$, $2.39 \sim 2.79$, $3.13 \sim 3.74$, and $4.69 \sim 5.34$ GHz. Besides, a new resonance point is generated at the first frequency band since the rectangular slots are introduced. There-

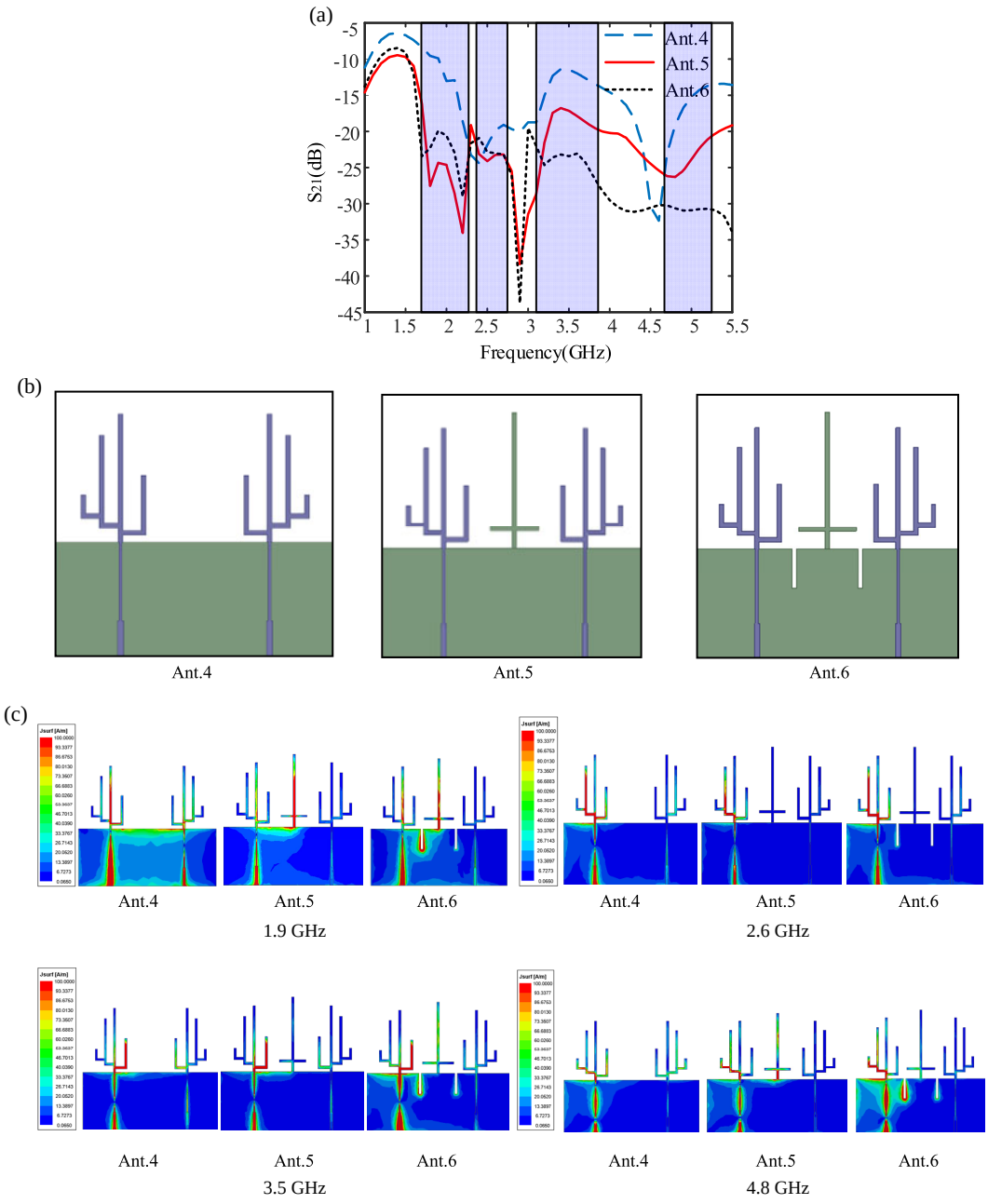

FIGURE 3. (a) The S_{21}-parameter curves of the quad-band MIMO antenna during decoupling stages. (b) Evolution procedures of the quad-band MIMO antenna decoupling. (c) Simulated current distributions of the quad-band MIMO antenna at 1.9, 2.6, 3.5 and 4.8 GHz during decoupling stages.

fore, the low-frequency bandwidth is widened to satisfy the demand of operating at the UMTS band.

Figure 5(c) provides the gain curves of the proposed antenna. When measuring the antenna gains, another standard horn antenna, termed as horn 2, is fabricated on the turntable in lieu of the prototype. The signal transmitted by the prototype and received by horn 1, is compared with the signal transmitted by horn 2 and received by horn 1. In this way, the gain of the prototype is obtained since the gain of horn 2 is known. From the measured results, it can be observed that the average gains at the four frequency bands are 3.72, 2.45, 2.13, and 2.24 dBi. In additional, a good agreement between the simulated and measured gain curves can be observed. The simulated and measured radiation efficiencies are given in Figure 5(d). As shown in Figure 5(d), it is seen that the simulated and measured antenna efficiencies are all better than 80%.

It is known that the envelope correlation coefficient (ECC) is provided to evaluate its MIMO performances. ECC is usually applied to quantify the correlation between the envelopes of the signals received by multiple antennas in a MIMO antenna system, which determines the similarity of the received signal amplitudes between different antenna elements. In practical scenarios, ECC values are preferred to remain below 0.5. As depicted in Figure 5(e), the simulated and measured values

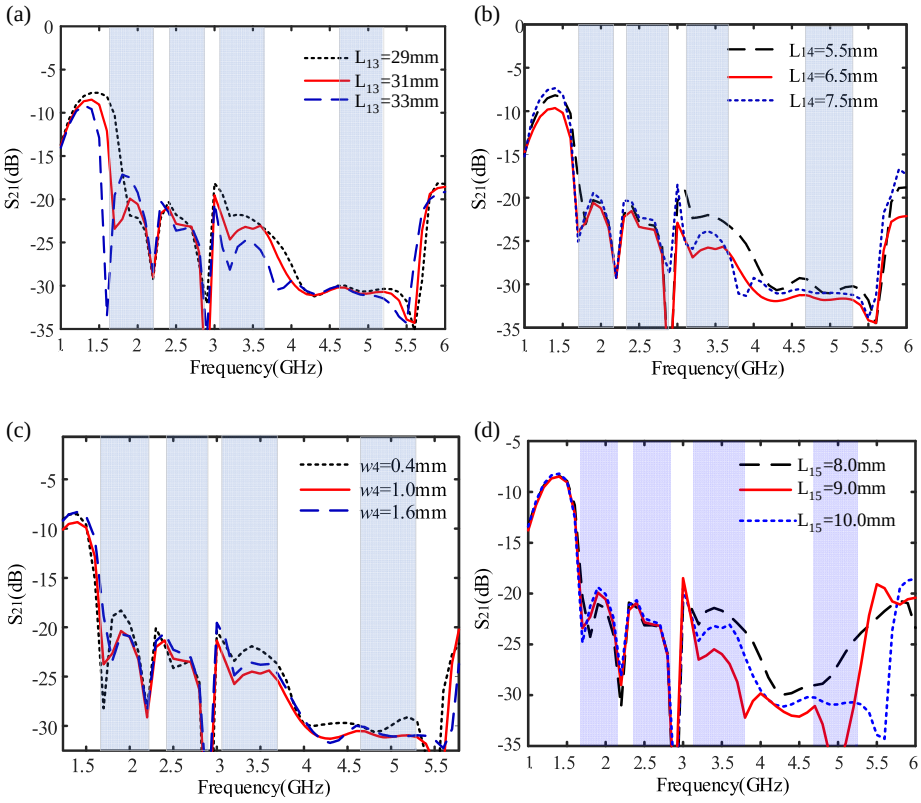

FIGURE 4. Simulated S_{21} with respect to (a) L_{13}, (b) L_{14}, (c) w_4, (d) L_{15}.

TABLE 1. Performance comparisons of the MIMO antennas.

Reference	No. of port	The center frequency (GHz)	Decoupling Method	Bandwidth (GHz)	Space (λ)	Isolation (dB)	Peak gain (dBi)	Efficiency (%)
[21]	8	4.63	strip and DGS	3.30–5.95	0.30	> 15	2.45	> 47
[22]	2	2.44, 5.49	resonant branch and T-shaped slot	2.40–2.48, 5.15–5.83	0.25	> 15	2.24, 2.15	> 78
[25]	4	3.50	Self-isolation	3.4–3.6	0.20	> 17	4.89	> 58
[26]	8	3.75, 4.90	Parasitic strip	3.3–4.2, 4.8–5.0	0.19	> 12.5	4.95, 3.42	> 53
[27]	4	3.5	Orthogonal polarization	3.4–3.6	—	> 12.9	3.79	> 39
[28]	2	3.44, 3.50	Differential feed	3.06–3.81, 3.33–3.67	0.28	> 14	5.17, 3.72	> 52
This work	2	1.98, 2.59 3.44, 5.02	Parasitic branch and DGS	1.67–2.28, 2.39–2.79, 3.13–3.74, 4.69–5.34	0.19	> 20	5.60, 3.38, 3.78, 4.41	> 80

of ECC between the two feed ports are less than 0.1 within the operating frequency bands, which means that a good ability of the interference suppression can be realized by the proposed antenna. The values of ECC from the measured S parameters are calculated using Eq. (1) [24]. The simulated and measured radiation patterns are presented in both E-plane and H-plane at 1.9, 2.6, 3.5, and 4.8 GHz as shown in Figure 5(f). During the measurement, the standard horn antenna is fixed in the same position while the prototype rotates with the turntable in horizontal plane. It should be highlighted that the prototype is placed horizontally and vertically on the turntable respectively for the measurement of patterns in E- and H-planes. As can be observed, it is seen that in the E-plane and H-plane, respectively, the proposed antenna exhibits approximately bidirectional and omnidirectional radiation at the four operating frequency points. Moreover, measured results are similar to the simulated ones within the operating bands.

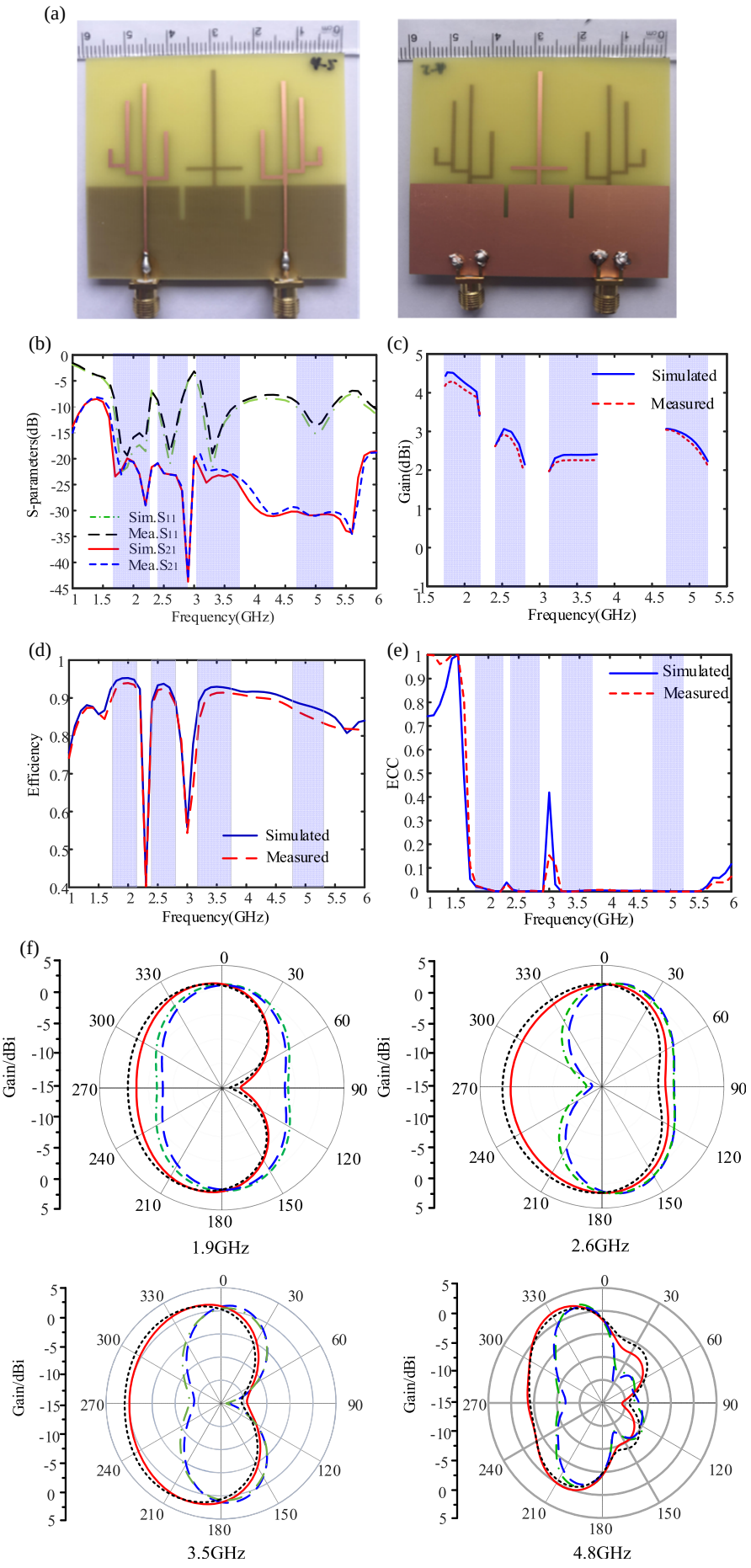
(a)
(b)
S-parameters(dB)
Sim.S11
Mea.S11
Sim.S21
Mea.S21
Frequency(GHz)
(c)
Gain(dBi)
Simulated
Measured
Frequency(GHz)
(d)
Efficiency
Simulated
Measured
Frequency(GHz)
(e)
ECC
Simulated
Measured
Frequency(GHz)
(f)
Gain/dBi
1.9GHz
2.6GHz
3.5GHz
4.8GHz

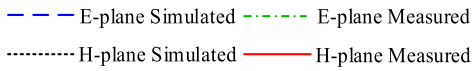

FIGURE 5. (a) Simulated antenna corresponding prototype. (b) Simulated and measured S-parameter. (c) Simulated and measured gains. (d) Simulated and measured total efficiencies. (e) Simulated and measured ECCs. (f) Simulated and measured radiation patterns.

Our work is compared with some recently reported MIMO antenna designs in Table 1. As can be observed, the majority of the designs cover less than two frequency bands. In our work, four frequency bands are realized, and a parasitic branch and DGS technologies are employed to enhance the isolation with the minimum element spacing. High isolation (> 20 dB) between two elements and better efficiency (80%) are obtained across the whole operating frequency bands.

$$\rho_e = \frac{\left|S_{11}^* S_{12} + S_{21}^* S_{22}\right|^2}{\left(1 - \left(\left|S_{11}\right|^2 + \left|S_{21}\right|^2\right)\right)\left(1 - \left(\left|S_{22}\right|^2 + \left|S_{12}\right|^2\right)\right)} \quad (1)$$

4. CONCLUSION

This letter presents a quad-band high-isolated MIMO microstrip antenna for coal mine communications. The proposed antenna can operate at four frequency bands of 1.67–2.28, 2.39–2.79, 3.13–3.74, and 4.69–5.34 GHz, which can cover the operating frequency regions of DCS1800/UMTS/WiMAX/WiFi/5G NR simultaneously. A qual-band element is firstly designed based on a quaddent structure which exhibits four resonant frequency points (1.9 GHz, 2.6 GHz, 3.5 GHz, and 4.8 GHz). Then the MIMO antenna is formed by symmetrically placing two quaddent structures with spacing of 0.19λ. To enhance the isolation level of the MIMO antenna, an inverted cross-shaped branch is loaded on and two rectangular slots are etched off the ground successively between the two elements. In this way, the isolation level is increased by more than 12 dB (from 8 dB to over 20 dB). A prototype is fabricated and measured. The results show that the proposed antenna has good MIMO performance and can completely cover DCS1800, UMTS, WiMAX, WiFi, and 5G NR ($1.67 \sim 2.28$ GHz, $2.39 \sim 2.79$ GHz, $3.13 \sim 3.74$ GHz and $4.69 \sim 5.34$ GHz). Therefore, the proposed antenna can become a good candidate in coal mine wireless communication.

ACKNOWLEDGEMENT

This work was supported in part by the National Natural Science Foundation of China under Grants No. 62271386, No. 61901357 and No. 62301415, and in part by the Shaanxi Provincial Association for Science and Technology Young Talents Trusteeship Program under Grant No. 20230149.

REFERENCES

[1] Dahlman, E., S. Parkvall, and J. Sköld, *5G NR: The Next Generation Wireless Access Technology*, Academic Press, New York, USA, 2018.

[2] Marcus, M. J., "5G and 'IMT for 2020 and beyond' [Spectrum Policy and Regulatory Issues]," *IEEE Wireless Communications*, Vol. 22, No. 4, 2–3, Aug. 2015.

[3] Xu, Y., Z. Zhang, A. Wang, and J. Hou, "Design of three multibranch microstrip antennas compatible with WiMAX/WiFi/4G/5G NR for coal mine applications," *Microwave and Optical Technology Letters*, Vol. 65, No. 3, 892–900, Mar. 2023.

[4] Varzakas, P., "Average channel capacity for rayleigh fading spread spectrum MIMO systems," *International Journal of Communication Systems*, Vol. 19, No. 10, 1081–1087, Dec. 2006.

[5] Zhang, Y.-M., Q.-C. Ye, G. F. Pedersen, and S. Zhang, "A simple decoupling network with filtering response for patch antenna arrays," *IEEE Transactions on Antennas and Propagation*, Vol. 69, No. 11, 7427–7439, Nov. 2021.

[6] Varzakas, P. and G. S. Tombras, "Spectral efficiency for a hybrid DS/FH code-division multiple-access system in cellular mobile radio," *IEEE Transactions on Vehicular Technology*, Vol. 50, No. 6, 1321–1327, Nov. 2001.

[7] Varzakas, P. and G. S. Tombras, "Comparative estimate of user capacity for FDMA and direct-sequence CDMA in mobile radio," *International Journal of Electronics*, Vol. 83, No. 1, 133–144, 1997.

[8] Janaswamy, R., "Effect of element mutual coupling on the capacity of fixed length linear arrays," *IEEE Antennas and Wireless Propagation Letters*, Vol. 1, 157–160, 2002.

[9] Li, G., H. Zhai, Z. Ma, C. Liang, R. Yu, and S. Liu, "Isolation-improved dual-band MIMO antenna array for LTE/WiMAX mobile terminals," *IEEE Antennas and Wireless Propagation Letters*, Vol. 13, 1128–1131, 2014.

[10] Rao, N. A. and L. B. Konkyana, "Four element MIMO antenna for wireless body area network and advanced wireless services applications," *Progress In Electromagnetics Research C*, Vol. 136, 151–160, 2023.

[11] Zhang, S. and G. F. Pedersen, "Mutual coupling reduction for UWB MIMO antennas with a wideband neutralization line," *IEEE Antennas and Wireless Propagation Letters*, Vol. 15, 166–169, 2016.

[12] Cai, J., J. Huang, B. Chen, L. Shen, T. H. Loh, and G. Liu, "A defected circular ring dual-band MIMO antenna with high isolation for 5G and IEEE 802.11 a/ac/ax," *Progress In Electromagnetics Research M*, Vol. 113, 237–247, 2022.

[13] Dkiouak, A., M. E. Ouahabi, S. Chakkor, M. Baghouri, A. Zakriti, and Y. Lagmich, "High performance UWB MIMO antenna by using neutralization line technique," *Progress In Electromagnetics Research C*, Vol. 131, 185–195, 2023.

[14] Song, W., X.-W. Zhu, L. Wang, and W. Hong, "Simple structure E-plane decoupled millimeter wave antenna based on current cancellation model," *IEEE Transactions on Antennas and Propagation*, Vol. 70, No. 10, 9871–9876, Oct. 2022.

[15] Khan, M. K. and Q. Feng, "A novel two port MIMO antenna having dual stopped-band functionality and enhanced isolation," *Progress In Electromagnetics Research M*, Vol. 113, 173–185, 2022.

[16] Gopal, K. V. and Y. S. Rao, "Mutual coupling reduction in UWB MIMO antenna using T-shaped stub," *Progress In Electromagnetics Research Letters*, Vol. 112, 77–85, 2023.

[17] Guo, J., F. Liu, L. Zhao, G.-L. Huang, W. Lin, and Y. Yin, "Partial reflective decoupling superstrate for dual-polarized antennas

application considering power combining effects," *IEEE Transactions on Antennas and Propagation*, Vol. 70, No. 10, 9855–9860, Oct. 2022.

[18] Liu, F., J. Guo, L. Zhao, G.-L. Huang, Y. Li, and Y. Yin, "Dual-band metasurface-based decoupling method for two closely packed dual-band antennas," *IEEE Transactions on Antennas and Propagation*, Vol. 68, No. 1, 552–557, Jan. 2020.

[19] Ye, Q.-C., Y.-M. Zhang, J.-L. Li, G. F. Pedersen, and S. Zhang, "High-isolation dual-polarized leaky-wave antenna with fixed beam for full-duplex millimeter-wave applications," *IEEE Transactions on Antennas and Propagation*, Vol. 69, No. 11, 7202–7212, Nov. 2021.

[20] Zhang, X.-K., Y.-H. Ke, X.-Y. Wang, S.-C. Tang, and J.-X. Chen, "Broadband dual-polarized dielectric patch antenna with high isolation for full-duplex communication," *IEEE Antennas and Wireless Propagation Letters*, Vol. 22, No. 4, 878–882, Apr. 2023.

[21] Hei, Y. Q., J. G. He, and W. T. Li, "Wideband decoupled 8-element MIMO antenna for 5G mobile terminal applications," *IEEE Antennas and Wireless Propagation Letters*, Vol. 20, No. 8, 1448–1452, Aug. 2021.

[22] Deng, J. Y., J. Li, L. Zhao, and L. Guo, "A dual-band inverted-F MIMO antenna with enhanced isolation for WLAN applications," *IEEE Antennas and Wireless Propagation Letters*, Vol. 16, 2270–2273, 2017.

[23] Xu, Y., P. Dong, and A. Wang, "Design of a high isolation tri-band MIMO antenna for coal mine applications," *Journal of Electromagnetic Waves and Applications*, Vol. 37, No. 13, 1106–1121, Sep. 2023.

[24] Sharawi, M. S., "Printed multi-band MIMO antenna systems and their performance metrics," *IEEE Antennas and Propagation Magazine*, Vol. 55, No. 5, 218–232, Oct. 2013.

[25] Ren, Z., A. Zhao, and S. Wu, "MIMO antenna with compact decoupled antenna pairs for 5G mobile terminals," *IEEE Antennas and Wireless Propagation Letters*, Vol. 18, No. 7, 1367–1371, Jul. 2019.

[26] Cui, L., J. Guo, Y. Liu, and C.-Y.-D. Sim, "An 8-element dual-band MIMO antenna with decoupling stub for 5G smartphone applications," *IEEE Antennas and Wireless Propagation Letters*, Vol. 18, No. 10, 2095–2099, Oct. 2019.

[27] Chang, L., Y. Yu, K. Wei, and H. Wang, "Polarization-orthogonal co-frequency dual antenna pair suitable for 5G MIMO smartphone with metallic bezels," *IEEE Transactions on Antennas and Propagation*, Vol. 67, No. 8, 5212–5220, Aug. 2019.

[28] Xu, Z. and C. Deng, "High-isolated MIMO antenna design based on pattern diversity for 5G mobile terminals," *IEEE Antennas and Wireless Propagation Letters*, Vol. 19, No. 3, 467–471, Mar. 2020.